Check for updates

Wiley
International Journal of Energy Research
Volume 2026, Article ID 2562219, 19 pages
https://doi.org/10.1155/er/2562219

WILEY

Research Article

Optimized FOPID-Controlled Wavelet Neural Network for Sensorless Speed Control of BLDC Motor Drive in Electric Vehicle Power Trains

D. S. Purushothaman,[1] **K. R. Santha**,[1] **Mohammed H. Alsharif**,[2] **and Mun-Kyeom Kim**[3]

[1]*Department of Electrical and Electronics Engineering, Sri Venkateswara College of Engineering, Chennai 602117, India*
[2]*Department of AI Convergence Electronic Engineering, Sejong University, Seoul 05006, Republic of Korea*
[3]*School of Energy System Engineering, Chung-Ang University, 84 Heukseok-ro, Dongjak-gu, Seoul 06974, Republic of Korea*

Correspondence should be addressed to D. S. Purushothaman; purush@svce.ac.in and Mun-Kyeom Kim; mkim@cau.ac.kr

Received 4 June 2025; Revised 18 July 2025; Accepted 10 September 2025

Guest Editor: Akshay Kumar Saha

Copyright © 2026 D. S. Purushothaman et al. International Journal of Energy Research published by John Wiley & Sons Ltd. This is an open access article under the terms of the Creative Commons Attribution License, which permits use, distribution and reproduction in any medium, provided the original work is properly cited.

Brushless direct current (BLDC) motors have become the preferred choice for electric vehicle (EV) power trains due to their exceptional performance attributes, including fast dynamic response, high efficiency, durability, low acoustic noise, and minimized electromagnetic interference (EMI), which is critical for applications sensitive to electrical noise. BLDC motors achieve precise electronic commutation via an inverter and a rotor position sensor; however, to reduce costs, sensorless control methods that estimate rotor position without physical sensors are often employed. This study presents an advanced control strategy for sensorless BLDC motor speed regulation using a wavelet neural network (WNN) optimized with a fractional-order proportional integral derivative (WNN-FOPID) controller. WNNs are well-suited for detecting intricate patterns in system data, enhancing control accuracy. The FOPID gains are optimally tuned using the random weighted chimp optimization (RW-CHO) algorithm, an enhanced version of the classic chimp optimization algorithm (ChOA). Performance evaluations demonstrate that the proposed approach achieves rapid settling (0.29343 s) and response times (0.24013 s), a control signal peak of 6250 within 0.02 s, indicating the maximum control output generated by the proposed system. It also shows a superior convergence rate (1.21% improvement), minimal error statistics (−1.487), and enhanced stability (rise time of 0.29249 s; settling time of 0.3625 s). Compared with existing techniques, the proposed WNN-FOPID-RW-ChOA model consistently achieves superior rotor speed control and precision, establishing a robust solution for sensorless BLDC motor applications in EVs.

Keywords: FOPID controller; random weighted chimp optimization algorithm; sensor less BLDC motor; wavelet neural network

1. Introduction

1.1. Background. Sensorless brushless direct current (BLDC) motors, which operate without hall effect sensors, provide a cost-effective solution for maintaining constant speeds and simplifying the rotor start-up process through electronic rotor position estimation. Recognized for their robust construction, low electromagnetic interference (EMI), and high power density, BLDC motors have gained popularity across a range of applications, including servo systems, actuation devices, positioning, and variable-speed drives [1, 2]. Traditional sensor-based BLDC motor drives, while precise, involve higher costs and potential reliability issues related to rotor position accuracy, making sensorless control strategies a practical and economical alternative [3]. BLDC motors fed by bipolar PWM inverters often experience commutation torque ripple; however, suitable commutation methods can help mitigate this issue [4, 5]. Sensorless BLDC motor control seeks to eliminate external sensors, reducing both system costs and complexity [6, 7]. Control strategies, such as PID controllers, and both nonadaptive and

adaptive fuzzy logic controllers (FLCs) have been proposed to optimize BLDC motor performance, ensuring precise operation without relying on sensor-based feedback [8, 9]. Although sensorless systems may face rotor position estimation challenges at higher speeds, they offer improved consistency and reduced steady-state energy losses [10, 11]. Incorporating FLCs into BLDC motor drives effectively addresses nonlinearities, boosting overall performance and robustness [12].

Advanced control methods, including PI and FLC controllers, have demonstrated efficacy in handling load variations and input fluctuations in BLDC drives [13]. To enhance speed regulation, conventional PID controllers have been upgraded to ANFIS models, improving response under dynamic conditions [14]. Additionally, a reverse electromotive force (EMF) detection–based approach has been introduced, providing precise rotor position estimation without sensors, thus, reducing complexity and cost [15]. Last, a sinusoidal PWM technique, renowned for simplicity and efficiency, has been implemented to regulate speed, while a sophisticated tuning system optimizes gain parameters, enhancing overall performance under varying load conditions [16, 17]. However, to overcome the challenges in sensorless speed control for BLDC motor drives in electric vehicles (EVs), promising techniques such as neural network (NN)–based approaches and fractional-order controllers offer potential solutions. Therefore, this work focuses on introducing an optimized control technique for sensorless speed control of BLDC motor drives in EVs, which may help in improving efficiency, accuracy, and overall performance.

1.2. Literature Review. In recent years, significant advancements in sensorless BLDC motor control strategies have been achieved, showcasing various methodologies to enhance speed regulation, precision, and robustness. A key development was proposed by Purushothaman and Santha [18] in 2022, introducing a sensorless BLDC motor drive system that uses an artificial NN (ANN) with a fractional-order proportional integral derivative (FOPID) controller, known as ANN-FOPID. ANNs are highly effective in pattern recognition, making them suitable for complex control tasks. This model leverages a random weighted chimp optimization (RW-CHO) algorithm to fine-tune FOPID controller parameters K_p, K_i, K_d, λ and μ, leading to enhanced speed regulation and control precision for sensorless BLDC drives.

Building upon this NN approach, Yao et al. [19] presented an ANN–based control algorithm for BLDC motors in 2023, using a multilayer perceptron (MLP) topology. This methodology further simplified control and improved rotor phase location and speed estimation by incorporating preconditioned phase voltage as input and utilizing encoder signals for training. Their results demonstrated the effectiveness of this approach in accurately estimating rotor position and speed, underscoring the value of NNs in BLDC motor control. In addition to NN–based approaches, fractional-order control techniques have also shown promising results. In 2022, Wang et al. [20] proposed a generalized proportional-fractional-order PI (GPFOPI) control algorithm optimized through a least squares optimization (LSO) technique. By integrating generalized analytical control with scalable fractional-order PI, the LSO-GPFOPI controller significantly outperformed conventional methods, offering enhanced rapidity tracking for BLDC motors.

Moving towards controllers specifically designed to improve torque and speed accuracy, Sayed et al. [21] introduced a tilt integral derivative (TID) controller in 2024. This controller effectively enhanced torque output and speed stability, providing promising results for applications requiring precise performance. For applications where noise reduction and smooth motor dynamics are critical, Kroičs and Būmanis [22] in 2024 implemented a fuzzy-based PID controller combined with an improved sinusoidal PWM technique. By incorporating third-harmonic distortion into the sine wave commutation, they were able to mitigate harmonics and reduce torque ripple, leading to a marked improvement in BLDC motor dynamics.

Addressing the need for sensorless solutions that still provide robustness under parameter uncertainties, Chandra et al. [23] proposed the SREH∞F strategy in 2023. This approach relies exclusively on electrical sensors to evaluate rotor position and mechanical states, making it a reliable option for managing parametric variations without mechanical sensors. In cases where turbulence and complex control environments challenge traditional controllers, advanced adaptive strategies have shown strong results. Rodríguez-Molina et al. [24] introduced a chaotic adaptive tuning strategy for controller gains (CATSCG) in 2022, which utilized a Lozi map-based chaotic initialization in the CODE algorithm to achieve precise gain adjustments. This two-phase optimization approach provided a robust method for handling turbulence and complex motor control requirements.

To further enhance performance in high-precision applications, Intidam et al. [25] in 2023 compared classical PI, PI-ANFIS, and particle swarm optimization (PSO)-PI-ANFIS controllers. Their findings indicated that the PSO-PI-ANFIS controller outperformed other methods by optimizing parameters through PSO, delivering heightened precision and responsiveness. These advancements collectively highlight a trend towards increasingly sophisticated and adaptive control methodologies, each addressing specific challenges in sensorless BLDC motor control, from pattern recognition and noise reduction to robustness against parameter uncertainties. Naqvi et al. [26] in 2023 have modeled the multiobjective optimization of BLDC motor speed control, energy usage, and efficiency using constrained differential evolution and particle swarm optimized PID controllers. The Ziegler–Nichols tuning method was applied to establish initial PI parameters, while real-time road gradient data was integrated into the EV control system to enhance precision and reduce energy consumption, especially on challenging roads. This approach significantly improved motor speed control and energy efficiency in EVs. Baba et al. [27] have modeled the speed control of a BLDC motor for EVs. Initially, the global model was simulated using MATLAB, with a PI controller ensuring speed control. Subsequently, PID and FLCs were implemented to achieve better performance, with each control method being compared based on the results obtained. The comparison highlighted the advantages of different control strategies in terms of speed regulation and overall system performance of BLDC motors in EVs. The following

ijer, 2026, 1, Downloaded from https://onlinelibrary.wiley.com/doi/10.1155/er/2562219 by MS HYEON - Chung-Ang University , Wiley Online Library on [11/03/2026]. See the Terms and Conditions (https://onlinelibrary.wiley.com/terms-and-conditions) on Wiley Online Library for rules of use; OA articles are governed by the applicable Creative Commons License

Table 1: Review of existing sensorless BLDC motor control strategies.

Author	Methodology	Advantages	Disadvantages
Purushothaman and Santha [18]	ANN–based RW-CHO	Enhanced speed control precision, handles nonlinear relationships	High computational load, prone to overfitting
Yao et al. [19]	MLP-ANN	Precise rotor position/speed estimation, robust system	High data dependency, lacks feature interpretability
Wang et al. [20]	LSO-GPFOPI	Fast response, resilience to interference	Gets stuck in local optima, limited convergence
Sayed et al. [21]	TID	Enhanced stability, lower steady-state offset	Sensitive to errors, high tuning complexity
Kroičs and Būmanis [22]	Fuzzy-based PID	Zero overshoot, rapid response, high-speed precision	Requires intensive tuning, sensitive to signal variations
Chandra et al. [23]	SREH∞F	Rapid target acquisition, stable control	Sensitive to nonlinearities, limited applicability
Rodríguez-Molina et al. [24]	CATSCG-CODE	Robust to perturbations, effective in complex environments	High analytical complexity, unpredictable fluctuations
Intidam et al. [25]	PSO-PI-ANFIS	Reduced overshoot, fast settling, computationally efficient	Susceptible to local minima, suboptimal control in some cases

comparison (Table 1) illustrates the trade-offs between advanced sensorless BLDC motor control strategies, highlighting how each approach addresses specific control requirements and limitations. Continued innovation in these methodologies will likely focus on improving robustness and computational efficiency to further enhance motor control accuracy across a variety of industrial applications.

1.3. Contributions. This research makes the following primary contributions:

- BLDC motors are widely preferred in EVs because due to their efficiency, high power density, and low maintenance requirements, reliability, and cost-effectiveness.
- Thus, this work presents a novel wavelet NN (WNN) integrated with an optimized FOPID controller, termed WNN-FOPID, designed to enhance precision in controlling the speed of sensorless BLDC motor drives in EVs. The WNN-FOPID approach leverages the adaptive learning capabilities of WNN to handle the dynamic and nonlinear characteristics of motor control, while the FOPID controller provides fine-tuned, fractional-order control adjustments for improved performance over traditional PID controllers.
- The study introduces the RW-CHO algorithm, an advanced optimization technique tailored to address a wide range of complex optimization problems. RW-CHO is engineered to enhance convergence speed and avoid common pitfalls, such as local optima trapping, by incorporating adaptive mechanisms that improve search efficiency. This makes it particularly effective in optimizing control parameters for motor speed regulation.
- The research thoroughly evaluates the effectiveness of the WNN-FOPID approach by comparing it with traditional control techniques across critical performance metrics. These include steady-state accuracy, transient response characteristics, and key parameters such as settling time and rise time. This comparative analysis highlights the advantages of WNN-FOPID in achieving faster response times and improved stability, demonstrating its potential as a superior control solution for sensorless BLDC motor drives.

The outline of this research is organized as follows: Section 2 presents the proposed WNN-FOPID-RW-CHO approach, discussing the sensorless BLDC motor drive in EVs and the implementation of the WNN and FOPID controller. Section 3 focuses on the optimization of the FOPID controller parameters using the RW-CHO algorithm. Section 4 details the simulation procedure, including performance analysis under various conditions. Finally, Section 5 concludes the study and discusses the results and future directions.

2. Proposed WNN-FOPID-RW-Chimp Optimization Algorithm (ChOA)

2.1. Sensorless BLDC Motor Drive. Brushless motors are electrically powered machines that operate without the need for brushes or commutators, utilizing alternating current (AC) to generate rotational motion. This AC power may be supplied directly or through an electronic circuit, which precisely controls the current's phase and frequency. Compared to traditional brushed motors, brushless motors offer notable advantages, such as enhanced efficiency, reduced weight, and higher performance. These benefits make brushless motors a popular choice for applications in robotics, drones, and automotive sectors, where reliability and energy efficiency are paramount [28]. The absence of brushes in brushless motors eliminates friction-related wear and tear, reducing the need for maintenance and extending operational life. Additionally, brushless motors can achieve a higher power output while effectively managing heat dissipation, making them ideal for high-demand applications where consistent performance is critical [29]. Among brushless motor types, BLDC motors are particularly valued for their high efficiency and torque density. However, they often require complex wiring setups

ijer, 2026, 1, Downloaded from https://onlinelibrary.wiley.com/doi/10.1155/er/2562219 by MS HYEON - Chung-Ang University , Wiley Online Library on [11/03/2026]. See the Terms and Conditions (https://onlinelibrary.wiley.com/terms-and-conditions) on Wiley Online Library for rules of use; OA articles are governed by the applicable Creative Commons License

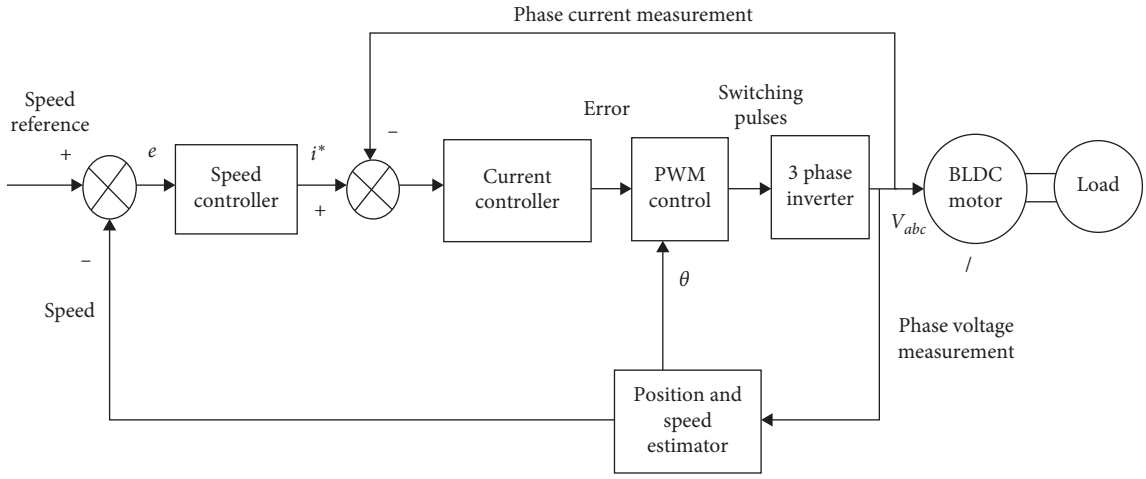


FIGURE 1: Schematic representation of a sensorless BLDC motor drive.

and rely on expensive rotor position sensors to function optimally. These sensors add to the motor's cost and can complicate installation, especially in compact or low-cost applications.

To address these challenges, sensorless BLDC drive systems have been developed as a cost-effective and efficient alternative. A sensorless drive system for BLDC motors aims to retain the motor's inherent advantages while enhancing both transient and steady-state performance. By eliminating the need for physical sensors, these systems simplify design and reduce costs [5]. Instead of sensors, sensorless systems utilize the trapezoidal back EMF generated by the rotating permanent magnet rotor to detect rotor position. This approach helps minimize fluctuations and noise commonly introduced by discrete sensors, leading to smoother and more accurate operation. In sensorless BLDC drives, critical parameters such as terminal voltage and current are monitored to estimate the motor's speed, flux, and torque, especially under varying load conditions. The real-time assessment of these parameters allows the system to adjust to changes quickly, maintaining optimal performance [30]. Intelligent control algorithms, often embedded in the motor's control system, play a key role in sensorless operation. These algorithms enable precise position estimation by processing motor variables, simplifying the evaluation process while maintaining high accuracy and efficiency [31]. Figure 1 illustrates a schematic of a sensorless BLDC motor drive, demonstrating how the drive system leverages back EMF feedback for effective rotor position estimation and control.

2.2. Speed Control of a Sensorless BLDC Motor in EVs Using WNN-FOPID. A power converter serves as a static device that converts a steady DC input into a variable AC signal by precisely managing switching elements based on pulse edges. In a BLDC motor system, the projected rotor position dictates whether these switches are activated or deactivated, thereby controlling the motor's rotational direction, speed, and torque. For sensorless BLDC motor control, the rotor speed is calculated indirectly through voltage and current measurements rather than physical sensors, which simplifies the design and reduces cost. The control process involves an error detector that compares the estimated rotor speed (ω)—obtained through the sensorless method—with a desired reference speed (ω_{ref}), which is manually set. This difference, or error signal, is processed by a WNN–based FOPID controller. The WNN-FOPID controller is specifically designed to handle the complexities of sensorless motor control, providing high precision and adaptability.

To optimize the FOPID controller's parameters, the RW-CHO algorithm is employed. RW-CHO is an improved version of the ChOA and is tailored to address the unique challenges of fine-tuning in high-precision applications like BLDC motor control. By iteratively adjusting the controller parameters, RW-CHO enhances the controller's response time and stability, ensuring efficient speed regulation even under varying load conditions. Figure 2 provides a schematic representation of the WNN-FOPID–based speed control system developed for sensorless BLDC motors in EVs. The diagram illustrates how the system integrates rotor position estimation, error detection, and optimized FOPID control, creating a robust framework for managing motor speed and performance in real time.

2.2.1. FOPID Controller. The FOPID controller, a closed-loop control system enhanced by feedback mechanisms, has become an essential tool for precise motor speed regulation and various process control applications. FOPID stands out due to its ability to enhance the dynamic performance of fractional-order controllers within closed-loop configurations, particularly beneficial in sensorless BLDC motor speed control. Unlike conventional PID controllers, FOPID offers two additional degrees of freedom, which provide greater control flexibility and fine-tuning capabilities. The FOPID controller's performance depends on its five primary parameters: proportional gain (K_p), integral gain (K_i), derivative gain (K_d), integral order (λ), and derivative order (μ). Each of these parameters is carefully adjusted to align the system output with the desired set point, ensuring accurate and consistent speed regulation [32]. The FOPID controller allows fine adjustments of the closed-loop system's time-domain and frequency-domain responses, including settling time, rise time, and peak time. This adjustability contributes

ijer, 2026, 1, Downloaded from https://onlinelibrary.wiley.com/doi/10.1155/er/2562219 by MS HYEON - Chung-Ang University , Wiley Online Library on [11/03/2026]. See the Terms and Conditions (https://onlinelibrary.wiley.com/terms-and-conditions) on Wiley Online Library for rules of use; OA articles are governed by the applicable Creative Commons License

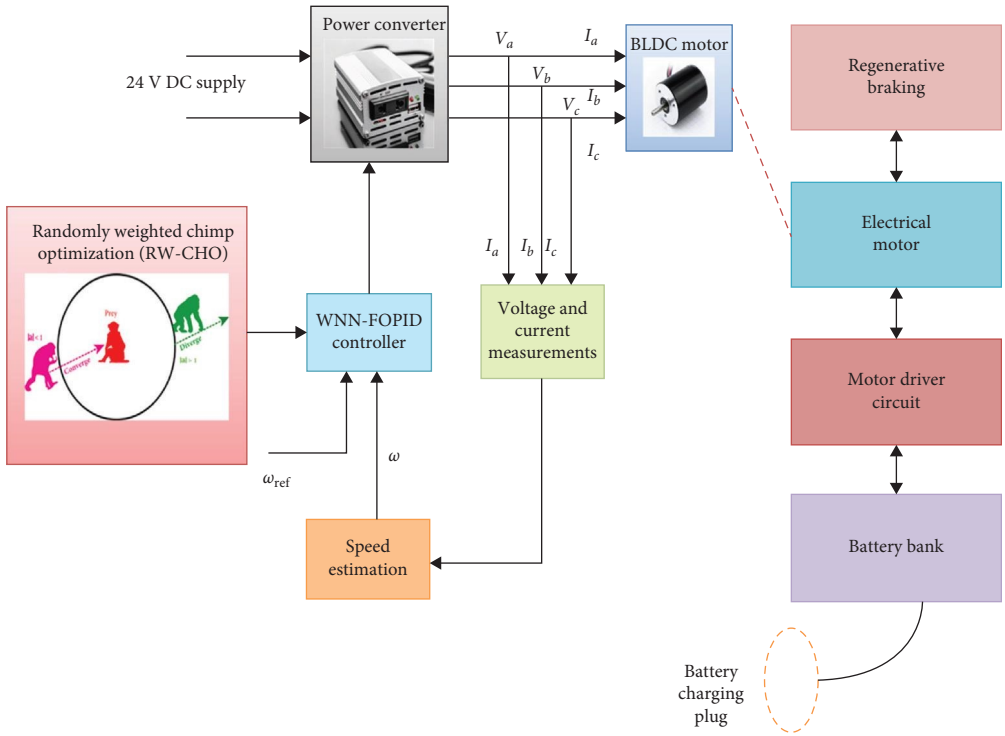


FIGURE 2: Schematic representation of developed WNN-FOPID–based speed control of sensorless BLDC motor in EVs.

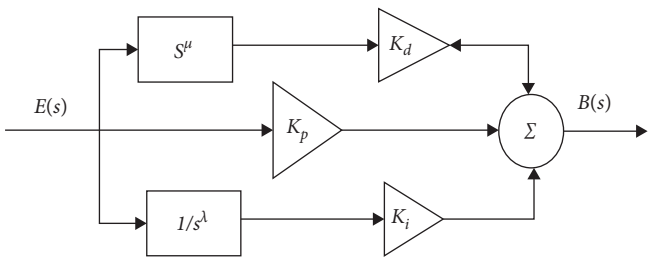


FIGURE 3: Architecture of FOPID controller.

to effective control over both transient and steady-state characteristics, making it ideal for high-precision applications like BLDC motor speed control [33].

In the proposed work, the FOPID controller's parameter tuning is optimized using the RW-CHO method, an enhanced ChOA variant. This optimization strategy minimizes key time-domain characteristics, such as rise time, peak time, settling time, and steady-state error, thereby improving both response speed and control accuracy. Figure 3 illustrates the basic structure of the FOPID controller within the system, showing how the controller interacts within the closed-loop configuration to regulate motor speed.

The transfer function G(s) of the PID controller is indicated in Equation (1).

$$G(s) = \frac{B(s)}{E(s)} = K_p + K_i s^{-\lambda} + K_d s^{\mu}, \tag{1}$$

where K_p is the proportional gain, K_i is the integral gain, K_d is the derivative gain and s is the laplace operator.

Time-domain representation of control signal is indicated as the general form of the FOPID controller is given by (Equation (2)):

$$B(t) = K_p E(t) + K_i D^{-\lambda} E(t) + K_d D^{\mu} E(t), \tag{2}$$

where $E(t)$ is the error signal and $D^{-\lambda}$ and $D^{-\mu}$ denotes the fractional integral operator, with fractional order λ and μ, respectively.

2.2.2. WNN. The wavelet transform is highly regarded for its time–frequency localization properties, making it particularly effective in analyzing signals with varying frequencies overtime. NNs, on the other hand, are valued for their self-adaptive capabilities, fault tolerance, and robust inferential power. Combining the strengths of both these methods—wavelet transform and NNs—has emerged as an important area of research in addressing complex real-world challenges. This integration is often referred to as a WNN or wavelet network (WN), which leverages the unique properties of wavelets to enhance the performance of NNs in various applications. In a WNN, the traditional Sigmoid activation function of a NN is replaced by a wavelet function. The choice of wavelet function brings with it the benefits of excellent time–frequency localization, making the network more capable of handling dynamic and non-stationary signals. The topology of a WNN is typically derived from the backpropagation (BP) network, where signals propagate forward through the network, and the errors are back-propagated during training. This structure allows the WNN to learn complex patterns and relationships in the data by adjusting the weights and biases in the network using a training algorithm and example data. As a result, WNNs can be tailored

ijer, 2026, 1, Downloaded from https://onlinelibrary.wiley.com/doi/10.1155/er/2562219 by MS HYEON - Chung-Ang University , Wiley Online Library on [11/03/2026]. See the Terms and Conditions (https://onlinelibrary.wiley.com/terms-and-conditions) on Wiley Online Library for rules of use; OA articles are governed by the applicable Creative Commons License

to specific problems based on the input–output relationships they are trained to capture, offering a high degree of flexibility and adaptability [34].

To minimize tracking errors, the WNN is trained to approximate the desired function by being exposed to a representative set of input–output patterns. The network is structured with multiple layers of neurons, including an input layer, one or more hidden layers, and an output layer. The performance of the WNN is highly dependent on the precision with which the weights are adjusted during the training process. The network learns to map the inputs to the desired outputs by minimizing the error between the predicted and actual outputs through weight updates in each iteration of training. This iterative adjustment helps the network optimize its performance for the given task [35]. For training, the developed approach utilizes 100 synthetic datasets containing randomly generated gain variables, along with the corresponding error measures obtained from the speed controller. These datasets serve as the training data for the WNN. During the training phase, the network adjusts its weights to minimize the error, ensuring that the WNN effectively learns to generate gain variables that correspond to zero error when tested. This process removes the element of randomness from the optimization, making the WNN more accurate and efficient in optimizing the control parameters. As a result, the WNN can effectively perform the optimization task and enhance the performance of the sensorless BLDC motor speed control system. WNNs are well suited for sensorless BLDC motor control due to their ability to capture time–frequency localization, handling nonlinear dynamics and noisy data efficiently. Unlike traditional NNs, WNNs adapt well to dynamic and varying motor conditions. The WNNs combined with FOPID controllers offer enhanced control accuracy and robustness.

3. Optimizing FOPID Controller Parameters Using RW-CHO Algorithm

3.1. Objective Model. To achieve optimal error reduction, this research focuses on fine-tuning the proportional (K_p), integral (K_i), and derivative (K_d) gain parameters, along with the fractional-order coefficients (λ and μ), within the FOPID controller. This optimization is designed to minimize the discrepancy between the actual rotor speed and the desired reference speed of the sensorless BLDC motor. By adjusting these parameters, the FOPID controller can achieve more precise and responsive speed control. The objective function for this optimization is formulated to quantify the error between the actual and desired motor speeds. The aim is to minimize this error by adjusting the controller's parameters. The proposed objective function is defined in Equation (4) as follows:

$$\text{Error} = \omega_{\text{ref}}(t) - \omega(t). \tag{3}$$

$$\text{Obj}_{\text{function}} = \text{Min error}. \tag{4}$$

This objective function is designed to penalize large errors and high derivatives, thereby encouraging smoother, more stable control. By minimizing error, the FOPID controller can achieve a balance between fast response times and minimal overshoot, resulting in better performance for the sensorless BLDC motor control system.

3.2. RW-CHO Algorithm. RW-CHO [1] is a newly developed meta-heuristic algorithm that is derived from the classical chimpanzee optimization algorithm [36]. It draws inspiration from the collective intelligence and sexual motivation observed in chimpanzees during hunting activities. The algorithm operates through four main stages—hunting, pursuing, blocking, and attacking—which mimic the behaviors and strategies employed by chimps in a hunting scenario. In the context of this work, the RW-CHO optimization method is employed for fine-tuning the parameters of the FOPID controller to achieve effective speed control for a sensorless BLDC motor drive. The optimization process helps to precisely adjust the proportional, integral, derivative, and fractional-order coefficients of the FOPID controller to minimize errors and improve the performance of the motor system.

The RW-CHO algorithm enhances the classical ChOA by introducing refinements in its approach, offering improved performance in solving complex optimization problems. Below is a breakdown of the stages involved in the classical ChOA, followed by the development and key features of the RW-CHO algorithm:

- Hunting: This stage simulates the initial search process, where chimpanzees explore the environment for potential prey. It represents the exploration phase of the algorithm, where the optimization process begins by searching the solution space randomly.
- Pursuing: Once a potential prey (solution) is located, the chimpanzees start pursuing it. This corresponds to the exploitation phase of the algorithm, where the focus is on refining and improving the solutions found in the hunting phase.
- Blocking: In this stage, the chimpanzees attempt to block the escape of their prey, symbolizing the algorithm's focus on constraining the search space by narrowing it down to more promising regions. This phase helps prevent premature convergence and ensures that the algorithm explores more potential solutions.
- Attacking: Finally, the chimpanzees attack the prey, ensuring that the solution is optimal. In the algorithm, this corresponds to the final optimization step, where the best possible solution is identified and refined.

The RW-CHO algorithm builds upon the classical ChOA by improving its efficiency and effectiveness in optimization tasks. Specifically, it uses an enhanced strategy for balancing exploration and exploitation, thereby achieving better performance in complex tasks such as tuning the FOPID controller parameters for sensorless BLDC motor control. By applying RW-CHO, this research aims to optimize the motor speed control process, achieving faster response times, reduced overshoot, and improved steady-state performance.

ijer, 2026, 1, Downloaded from https://onlinelibrary.wiley.com/doi/10.1155/er/2562219 by MS HYEON - Chung-Ang University , Wiley Online Library on [11/03/2026]. See the Terms and Conditions (https://onlinelibrary.wiley.com/terms-and-conditions) on Wiley Online Library for rules of use; OA articles are governed by the applicable Creative Commons License

3.2.1. Strategy of Pursuing and Hunting the Prey. In the RW-CHO algorithm, the behaviors of chimpanzees during the exploration and exploitation stages—specifically, during the pursuing and attacking phases—are modeled using mathematical equations to guide the search for optimal solutions. These stages are designed to simulate how chimpanzees pursue and capture prey in the wild, to refine the optimization process. Below are the statistical representations of driving the prey and chasing the prey behaviors, which are described by Equations (5) and (6):

$$F = \left|D \cdot Y_p(\text{itr}) - N \cdot Y_c(\text{itr})\right|. \tag{5}$$

$$Y_c(\text{itr}+1) = Y_p(\text{itr}) - B \cdot F. \tag{6}$$

In these equations, B, N, and D are constant vectors, while Y_p and Y_c denote the vector location of the prey and the chimp, respectively, and F represents the adaptive control parameter. The vectors B, N, and D are determined by Equations (7), (9), and (10), respectively.

$$B = 2 \cdot H \cdot z_1 - H. \tag{7}$$

RW-CHO employs an exponential decay function to dynamically adjust the variable h throughout the optimization process:

$$H = 2 \cdot \left(1 - \left(\frac{\text{itr}^2}{\text{itr}_{\max}^2}\right)\right), \tag{8}$$

where iter depicts the current iterations and T indicates the maximum iterations.

$$D = 2 \cdot z_2. \tag{9}$$

$$n = \text{Chaotic}_{-\text{value}}. \tag{10}$$

At the time of the exploitation and exploration stages, the random vectors x_1 and x_2 are confined to the range [0, 1]. Finally, a chaotic vector n is generated using the distinct chaotic map.

3.2.2. Attacking Strategy (Phase of Exploitation). The chimp identifies the prey's current position through a sequence of actions, such as driving, blocking, and chasing, ultimately encircling the prey. In the hunting process, the attacker chimps are responsible for the direct pursuit, while the drivers, barriers, and chasers assist in the hunt. When mathematically modeling chimp behavior, it is assumed that the primary attacker (representing the best solution), along with the driver, barrier, and chaser, all have an enhanced awareness of the potential prey's location, which is determined by equations Equation (11) and (12). As a result, the best solutions found are recorded and updated based on the position of the optimal chimp.

$$F^{\text{attacker}} = \left|D_1 Y^{\text{attacker}} - N_1 Y\right| \text{ and } F^{\text{barrier}} = \left|D_2 Y^{\text{barrier}} - N_2 Y\right|. \tag{11}$$

$$Y_1 = Y^{\text{attacker}} - B_1\left(F^{\text{attacker}}\right) \text{ and } Y_2 = Y^{\text{barrier}} - B_2\left(F^{\text{barrier}}\right),$$

$$Y_3 = Y^{\text{chaser}} - B_3\left(F^{\text{chaser}}\right) \text{ and } Y_4 = \left(Y^{\text{driver}}\right) - B_4\left(F^{\text{driver}}\right). \tag{12}$$

Based on the prey's position, four weighting factors are introduced, each corresponding to a random value such that their sum equals 1. This leads to the updated chimp position being determined by the RW-CHO algorithm.

$$Y(\text{itr}+1) = \frac{M_1 Y_1 + M_2 Y_2 + M_3 Y_3 + M_4 Y_4}{4}, \tag{13}$$

where Y_1, Y_2, Y_3, and Y_4, are the difference between chimp drives, where Y_1 is highly significant probability, Y_2 less significant probability than Y_1, Y_3 lower probability than Y_2, and Y_4 lower probability than Y_3. The probabilities associated with these values can be adjusted depending on the importance of the problem being solved.

Equation (13) illustrates the RW-CHO Algorithm. Here, $M_1 = 0{:}4$, $M_2 = 0{:}35$, $M_3 = 0{:}1$, and $M_4 = 0{:}1$ and $M_1 + M_2 + M_3 + M_4 = 1$.

3.2.3. Predation (Utilization Phase). In the final phase, the chimps continue to engage the prey until it ceases to move, marking the end of the process. To mathematically model this attack and hunting phase, the variable is progressively reduced, with the range of variance for this variable specified. Over the course of iterations, the random variable is defined by the functions $-2H$, H, and B, where H decreases from 2.5 to 0. The random values of B are constrained within the range of -1, and as a result, the next position of the chimp will lie between its current location and the prey's location.

3.2.4. Prey Search (Exploration Phase). Exploration within the chimp groups involves the positions of the attacker, barrier, chaser, and driver chimps. This process unfolds in two main stages: the divergence stage, where the chimps search for the prey, and the convergence phase, where they focus on attacking the prey. To characterize the performance of these stages, if the vector B takes a random value greater than 1 or less than -1, the search agent is compelled to move away from the prey. This strategy facilitates the exploration process, enabling the chimp to conduct a wider and more thorough search.

3.2.5. Social Influence (Reproductive Drive). As mentioned earlier, in the final stage, the increased social motivation leads the chimp to abandon its previous responsibilities, causing it to search for food more erratically. This chaotic behavior helps the chimpanzees avoid getting trapped in local optima and accelerates the convergence process. It is assumed that there is a 50% chance of selecting between the standard update location and a chaotic model for updating the chimps' position in the optimization process. This mechanism is described by the

ijer, 2026, 1, Downloaded from https://onlinelibrary.wiley.com/doi/10.1155/er/2562219 by MS HYEON - Chung-Ang University , Wiley Online Library on [11/03/2026]. See the Terms and Conditions (https://onlinelibrary.wiley.com/terms-and-conditions) on Wiley Online Library for rules of use; OA articles are governed by the applicable Creative Commons License

Initiate the population of chimp
Initiate *H*, *N*, *B* and *D*
Compute every location of chimp
Evaluate fitness function of every chimp
Choose the most effective search agent for the roles of attacker, chaser, barrier, and driver
while ($itr < itr_{max}$)
for **each chimp**
  Describe the set of chimps
    Upgrade *H*, *N* and *D* by means of group approach
  Compute B and F
end for
for **each search chimp**
if ($\phi < 0.5$)
if ($|B| < 1$)
    Upgrade the present position of chimp using Equation (6)
else if ($|B| < 1$)
Choose a search agent at random
end if
else if ($\phi > 0.5$)
    Upgrade the present position of chimp using Equation (14)
Upgrade *H*, *N*, *B* and *D*
Upgrade $Y^{attacker}$, $Y^{barrier}$, Y^{chaser}, Y^{driver}
    Update Z_s^* if an optimal position exists
$itr = itr + 1$
  end while
Return $Y^{attacker}$

Algorithm 1: Pseudo code of RW-CHO technique.

corresponding Equation (14), where (r) is a random number in the range [0,1].

$$Y_c(\text{itr}+1) = \begin{cases} Y_p(\text{itr}) - B \cdot F & \text{if } \phi < 0.5 \\ \text{Chaotic_value} & \text{if } \phi > 0.5 \end{cases}. \quad (14)$$

Algorithm 1 provides the pseudo code of the RW-CHO algorithm. The flowchart illustrating the developed RW-CHO algorithm is shown in Figure 4.

4. Results and Discussions

4.1. Simulation Procedure. The proposed WNN-FOPID–based speed controller for sensorless BLDC motor drives is implemented and tested in MATLAB/Simulink, with experimental validation. The performance of the proposed WNN + PROP model was compared to existing methods, including RW-CHO [1], WNN [35], WNN + LI, and WNN + PSO [12]. The ChOA, which is a meta-heuristic optimization technique inspired by the hunting behaviors of chimpanzees, is known for its effectiveness in exploring complex, multi-dimensional optimization problems. Additionally, the WNN, which integrates wavelet transforms to enhance the ability of NNs. The lion algorithm (LI), inspired by the social behaviors and hunting strategies of lions, was also compared for its balance of exploration and exploitation in optimization tasks. Finally, PSO [12], which simulates the social behavior of birds, was compared for its global search capability in optimization. Both loaded and unloaded conditions were considered to evaluate the speed response of the BLDC motor drives. Table 2 depicts the system parameters used for simulation.

4.2. Speed Analysis

4.2.1. Analysis of Speed Under Load Conditions. Figure 5 presents a comparative analysis of the speed responses of the proposed WNN + PROP model against traditional models, including RW-CHO, WNN, WNN + LI, and WNN + PSO. The comparison was conducted at a reference speed of 300 rpm under three different torque loads: 10, 5, and 8 N m. The simulation was carried out within a speed range of 0–350 rpm and a time span of 0–0.6 s. The results reveal that the proposed WNN + PROP model achieved a settling time of 0.36252 s under a 10 N m torque load, which was notably faster than the traditional methods. Specifically, RW-CHO had a settling time of 0.36321 s, WNN exhibited 0.36865 s, WNN + LI showed 0.36478 s, and WNN + PSO demonstrated 0.36325 s. This improvement in settling time highlights the effectiveness of the WNN + PROP model in achieving faster response times under higher torque load conditions.

ijer, 2026, 1, Downloaded from https://onlinelibrary.wiley.com/doi/10.1155/er/2562219 by MS HYEON - Chung-Ang University , Wiley Online Library on [11/03/2026]. See the Terms and Conditions (https://onlinelibrary.wiley.com/terms-and-conditions) on Wiley Online Library for rules of use; OA articles are governed by the applicable Creative Commons License

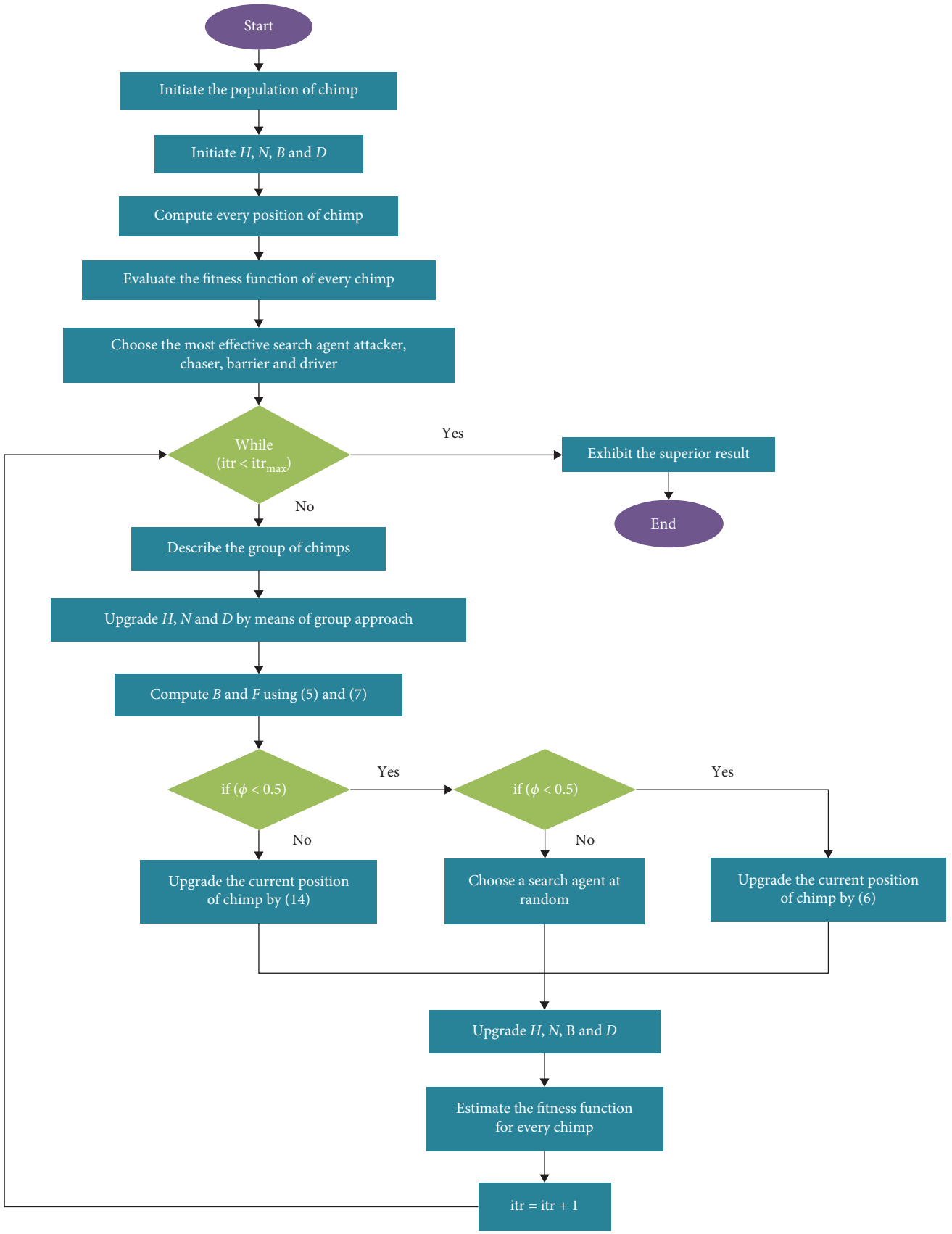


Figure 4: Flowchart of RW-CHO.

ijer, 2026, 1, Downloaded from https://onlinelibrary.wiley.com/doi/10.1155/er/2562219 by MS HYEON - Chung-Ang University , Wiley Online Library on [11/03/2026]. See the Terms and Conditions (https://onlinelibrary.wiley.com/terms-and-conditions) on Wiley Online Library for rules of use; OA articles are governed by the applicable Creative Commons License

Table 2: System parameters used for simulation.

Brushless DC motor drive	
Resistance (ohm)	0.2
Inductance (H)	$8.5e^{-3}$
Back EMF flat area (°)	120
Flux constant	0.175
Inertia (kg m^2)	0.089
Friction factor (N m s)	0.005
Pole pairs	4
Capacitance (F)	$2000e^{-6}$
Resistance (ohm)	8
Chopper frequency (Hz)	4000
Activation voltage (V)	320
Shutdown voltage (V)	310
Inverter	
Snubber resistance, R_s (Ohms)	500
Snubber capacitance, C_s (F)	$1e^{-6}$

When tested under a 5 N m torque load, the proposed technique showed a slightly improved settling time of 0.29318 s, outperforming the other benchmark methods. For instance, WNN had a settling time of 0.29345 s, WNN + LI had 0.29327 s, and WNN + PSO showed 0.29338 s. These minor yet significant differences indicate that the WNN + PROP model is more responsive under moderate torque conditions as well. Furthermore, under an 8 N m torque load, the WNN + PROP model demonstrated a settling time of 0.29343 s, surpassing the performance of the traditional approaches. For comparison, WNN showed a settling time of 0.29353 s, WNN + LI had 0.29336 s, and WNN + PSO exhibited 0.29348 s. This further confirms the WNN + PROP model's ability to deliver faster responses under varying torque load conditions.

4.2.2. Analysis of Speed Under No-Load Condition. Figure 6 presents a comparison of the speed responses between the conventional RW-CHO, WNN, WNN + LI, and WNN + PSO methods and the proposed WNN + PROP model under no-load conditions, with a reference speed of 300 rpm. The speed range for the simulation was 0–350 rpm, and the time span was 0–0.6 s. The results reveal that the traditional methods, including RW-CHO, WNN, WNN + LI, and WNN + PSO, achieved rise times of 0.24018, 0.24062, 0.24019, and 0.24017 s, respectively. In contrast, the proposed WNN + PROP model exhibited a notably faster rise time of 0.24013 s, indicating a quicker response in reaching the desired speed. These simulation results clearly demonstrate that the WNN + PROP method outperforms the conventional approaches in terms of rise time, highlighting its superior speed control performance under no-load conditions. The faster response of the WNN + PROP model confirms its effectiveness in optimizing the speed regulation of sensorless BLDC motor drives compared to traditional methods.

4.3. Control Signal Analysis With and Without Load. Figure 7 presents a comparative analysis of the control signal behavior for the proposed WNN + PROP technique and traditional methods under varying torque loads. Under a 10 N m torque load, the proposed WNN + PROP method reaches a maximum control signal of 2750 at 0.2 s, surpassing the traditional approaches in both peak amplitude and response time. For lighter loads of 5 and 8 N m, the proposed method attains maximum control signal values of 2500 and 6250, respectively, at notably shorter time intervals of 0.15 and 0.02 s. These results demonstrate the superior responsiveness and control efficiency of the proposed WNN + PROP method. The significantly faster response times under different torque loads highlight the method's ability to adapt more effectively to dynamic conditions, offering improved performance compared to traditional techniques such as WNN, WNN + LI, and WNN + PSO. This makes the WNN + PROP approach more suitable for real-time control applications where rapid and precise adjustment of the control signal is critical.

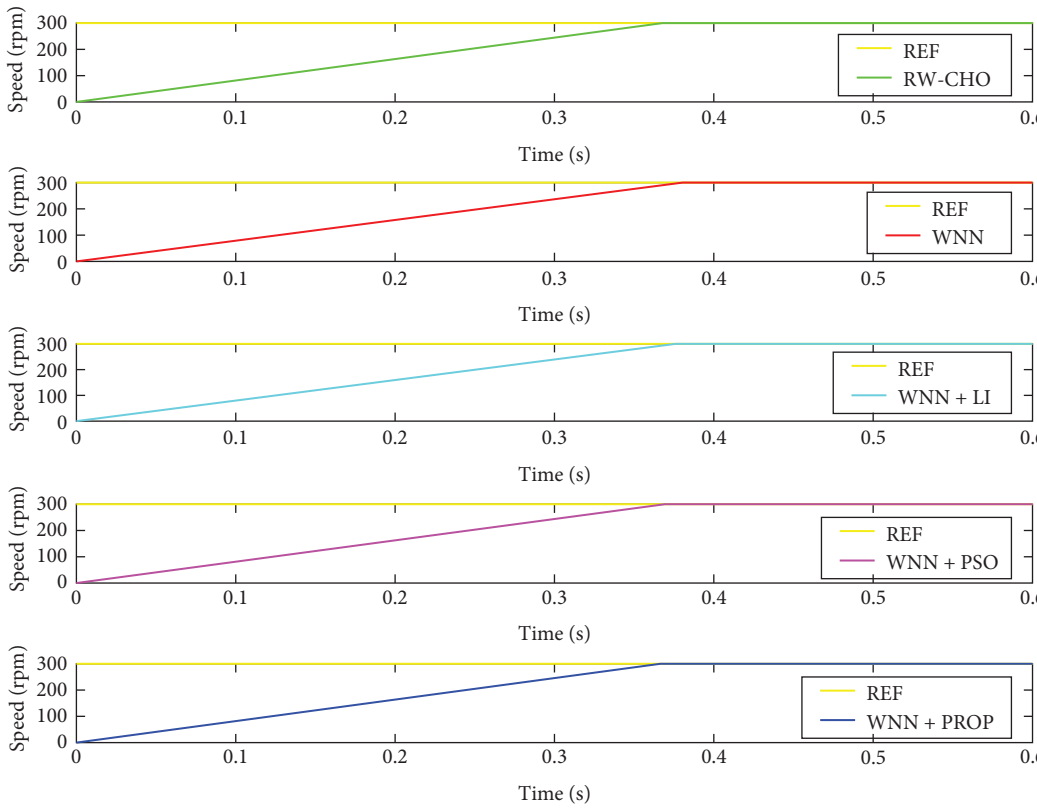
Figure 8 showcases the enhanced control signal response of the proposed WNN + PROP method under no-load conditions. The WNN + PROP technique reaches a peak control signal of 4500 in just 0.13 s, significantly outperforming the traditional methods in both amplitude and response time. This rapid response highlights the effectiveness of the proposed approach in achieving quick and precise control, further emphasizing its superiority over conventional methods in dynamic, no-load situations. The faster rise time and higher peak amplitude illustrate the method's potential for real-time applications that demand high-performance control.

4.4. Convergence Analysis. Figure 9 illustrates the convergence rates of the proposed WNN + PROP model compared to traditional methods, namely, WNN + LI and WNN + PSO, under both loaded and unloaded conditions. The results highlight the faster convergence of the WNN + PROP technique relative to the conventional approaches. Under load conditions, at the 5th iteration, the proposed method converged 1.38% and 0.06% faster than WNN + LI and WNN + PSO, respectively. At the 10th iteration, WNN + PROP exhibited a 1.06% and 0.25% faster convergence compared to WNN + LI and WNN + PSO.

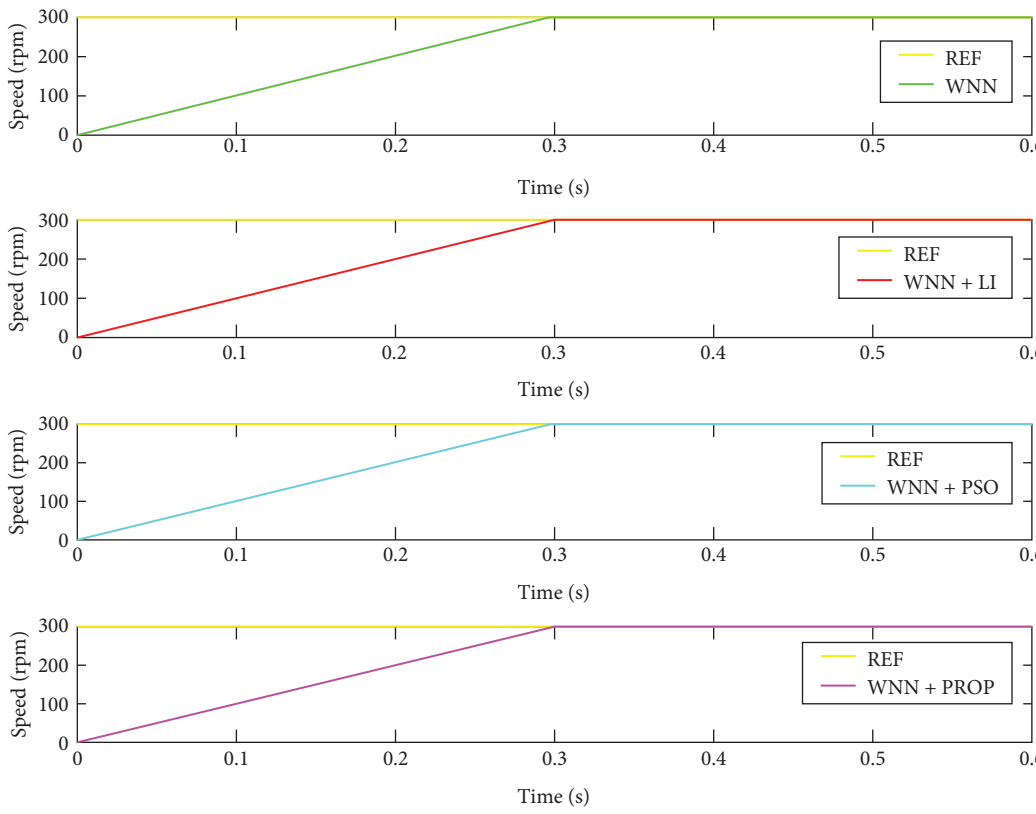
The proposed WNN + PROP method's superiority in convergence speed was also evident under no-load conditions, where at the 15th iteration, it outperformed WNN + LI and WNN + PSO, showing a 0.25% and 1.21% improvement in convergence speed, respectively. Furthermore, at the 20th iteration, WNN + PROP continued to maintain its advantage, converging 0.25% and 1.21% faster than WNN + LI and WNN + PSO, respectively. These simulation results underscore the efficiency of the WNN + PROP method, demonstrating its consistent ability to achieve faster convergence than the traditional techniques under both loaded and unloaded scenarios.

4.5. Error Statistics. Table 3 presents the error statistics for a 10 N m torque load, highlighting the superior performance of the proposed WNN + PROP method. The proposed approach achieves a minimum error of −1.487, outperforming the traditional methods. Specifically, the RW-CHO method yields an error of −1.479, WNN results in −1.554, WNN + LI produces −1.456, and WNN + PSO shows an error of −1.498. These results demonstrate that the proposed WNN + PROP method offers a lower error margin, indicating better precision and

ijer, 2026, 1, Downloaded from https://onlinelibrary.wiley.com/doi/10.1155/er/2562219 by MS HYEON - Chung-Ang University , Wiley Online Library on [11/03/2026]. See the Terms and Conditions (https://onlinelibrary.wiley.com/terms-and-conditions) on Wiley Online Library for rules of use; OA articles are governed by the applicable Creative Commons License



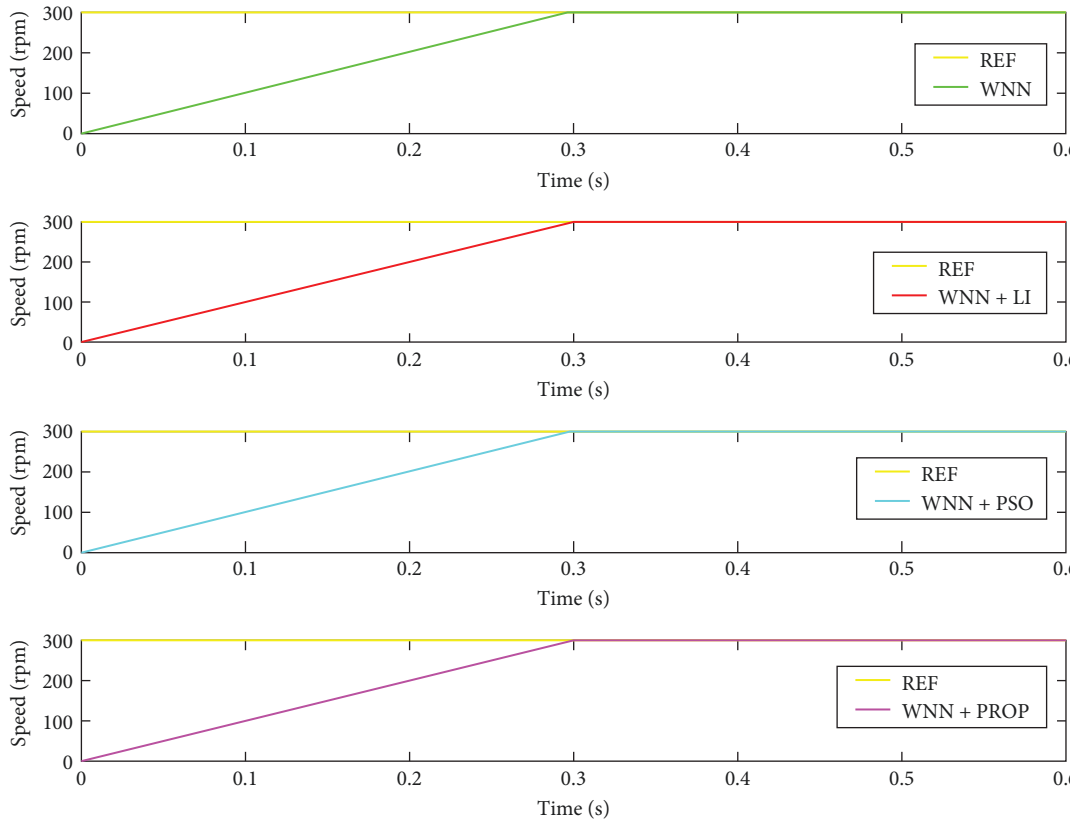
(a)



(b)

Figure 5: Continued.

ijer, 2026, 1, Downloaded from https://onlinelibrary.wiley.com/doi/10.1155/er/2562219 by MS HYEON - Chung-Ang University , Wiley Online Library on [11/03/2026]. See the Terms and Conditions (https://onlinelibrary.wiley.com/terms-and-conditions) on Wiley Online Library for rules of use; OA articles are governed by the applicable Creative Commons License



(c)

FIGURE 5: Comparative analysis of speed under load conditions. (a) Torque load at 10 N m. (b) Torque load at 5 N m. (c) Torque load at 8 N m.

accuracy in speed control compared to the conventional techniques.

Table 3 presents the error statistics for torque loads of 5 and 8 N m, showcasing the performance of the proposed WNN + PROP method. Under a 5 N m torque load, the proposed method achieves a slightly lower error of 302.36, outperforming the traditional methods: WNN with 302.32, WNN + LI with 302.41, and WNN + PSO with 302.41. At an 8 N m torque load, the proposed method further demonstrates its superiority, achieving a mean error value of 224.65, compared to WNN with 224.92, WNN + LI with 224.72, and WNN + PSO with 224.98. These results highlight the effectiveness of the WNN + PROP method in minimizing error, offering improved accuracy in speed control under different torque loads compared to conventional techniques.

Table 4 presents the error statistics under no-load conditions, comparing the proposed WNN + PROP method with traditional techniques. The proposed method achieves a standard deviation (STD) of 96.472, which is consistent with the results of the conventional methods. Specifically, the traditional methods—RW-CHO, WNN, WNN + LI, and WNN + PSO—each also report STD of 96.472. These results indicate that, under no-load conditions, the proposed WNN + PROP method performs similarly to the traditional methods in terms of error deviation, maintaining a comparable level of stability and accuracy.

4.6. Stability Analysis. To assess the stability of the proposed WNN + PROP method, a range of time-domain metrics were analyzed, including rise time, settling time, settling minimum, settling maximum, overshoot, undershoot, peak value, and peak time. Table 5 summarizes the results of the stability analysis under a 10 N m torque load. The proposed technique exhibits a rise time of 0.29249 s, outperforming the traditional methods. Specifically, RW-CHO recorded a rise time of 0.29281 s, WNN took 0.29676 s, WNN + LI required 0.29436 s, and WNN + PSO achieved 0.29228 s. These results highlight the faster initial response of the proposed WNN + PROP method.

Additionally, the proposed approach demonstrates a settling time of 0.36252 s, which is significantly shorter than the traditional methods: RW-CHO (0.36321 s), WNN (0.36865 s), WNN + LI (0.36478 s), and WNN + PSO (0.36325 s). This indicates that the proposed method not only reaches its steady state more quickly but also maintains superior stability over the other approaches. These findings underscore the enhanced performance of the WNN + PROP method, both in terms of faster response and improved stability, making it a more effective solution for controlling sensorless BLDC motors under load conditions.

Table 5 presents the results of the stability analysis under a 5 N m torque load condition. The proposed WNN + PROP method achieves a minimum settling time of 270.05 s, which

ijer, 2026, 1, Downloaded from https://onlinelibrary.wiley.com/doi/10.1155/er/2562219 by MS HYEON - Chung-Ang University , Wiley Online Library on [11/03/2026]. See the Terms and Conditions (https://onlinelibrary.wiley.com/terms-and-conditions) on Wiley Online Library for rules of use; OA articles are governed by the applicable Creative Commons License

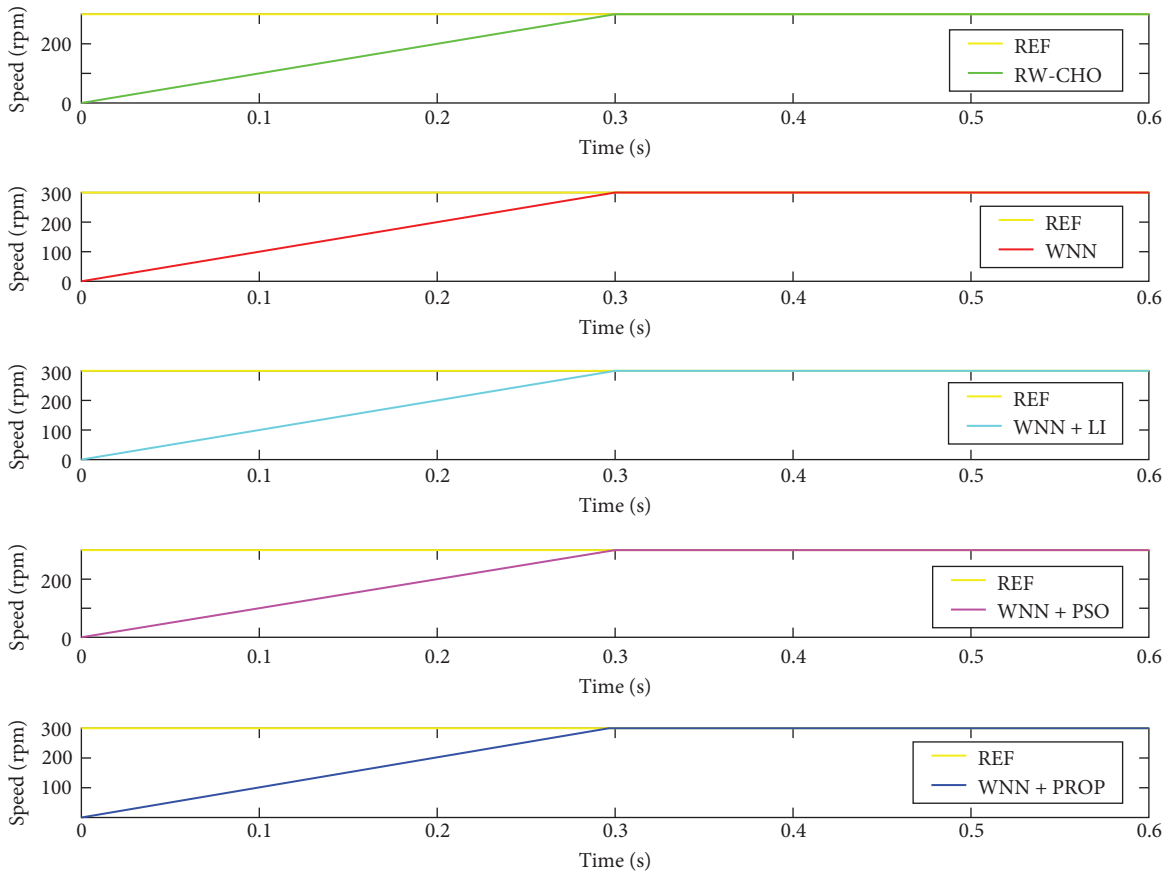


Figure 6: Comparative speed analysis under no-load condition.

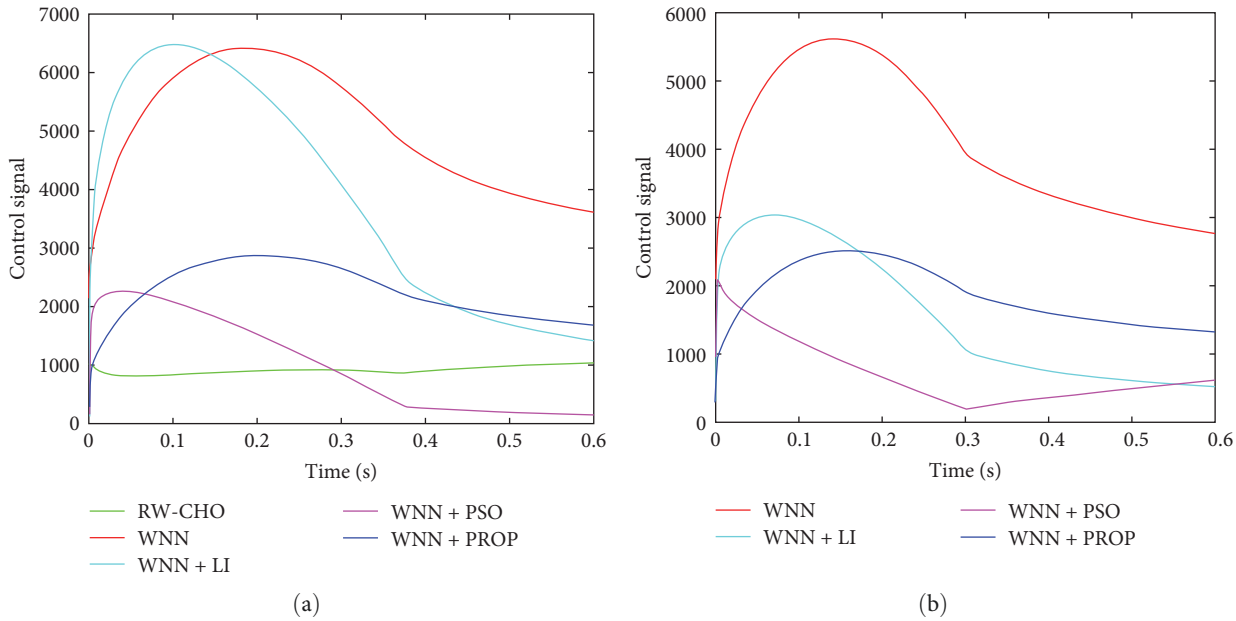
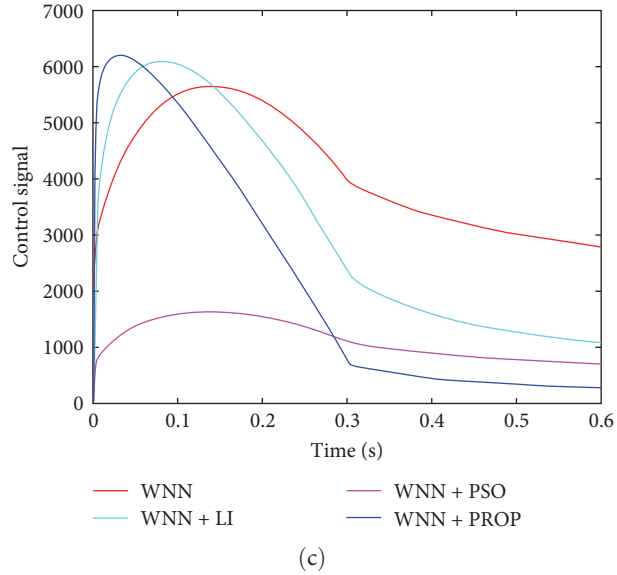


Figure 7: Continued.

ijer, 2026, 1, Downloaded from https://onlinelibrary.wiley.com/doi/10.1155/er/2562219 by MS HYEON - Chung-Ang University , Wiley Online Library on [11/03/2026]. See the Terms and Conditions (https://onlinelibrary.wiley.com/terms-and-conditions) on Wiley Online Library for rules of use; OA articles are governed by the applicable Creative Commons License



(c)

FIGURE 7: Control signal performance comparison with load. (a) Torque load at 10 N m. (b) Torque load at 5 N m. (c) Torque load at 8 N m.

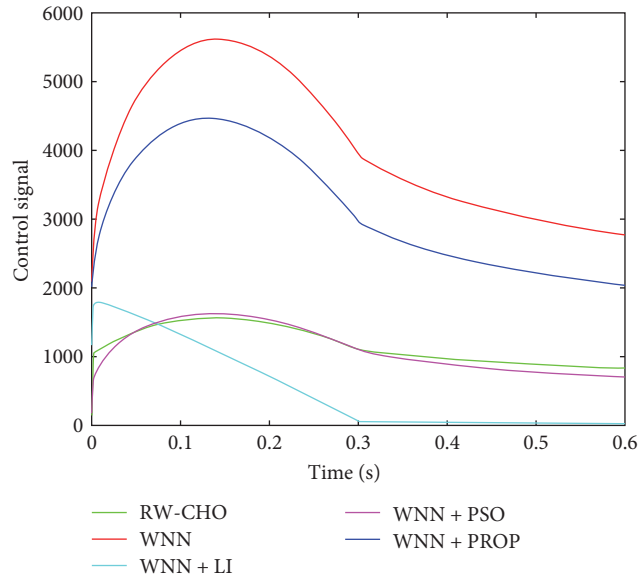


FIGURE 8: Control signal performance comparison without load.

is notably superior to the traditional methods. Specifically, the WNN method requires 270.06 s, WNN + LI takes 270.06 s, and WNN + PSO requires 270.12 s. This demonstrates that the proposed approach achieves a quicker stabilization time compared to the conventional techniques. Furthermore, the maximum settling time for the proposed method is 302.36 s, while the traditional methods show slightly longer settling times: WNN takes 302.32 s, WNN + LI requires 302.41 s, and WNN + PSO also reaches 302.41 s. These results emphasize the superior timing performance of the proposed WNN + PROP method, illustrating its ability to stabilize more efficiently than the existing methods under a 5 N m torque load.

Table 5 presents the stability analysis results under an 8 N m torque load. The proposed WNN + PROP method demonstrates a significantly lower overshoot of 0.8329 s, which is much smaller than the overshoot observed in traditional methods. Specifically, the WNN method exhibits an overshoot of 73.136 s, WNN + LI shows 4.3315 s, and WNN + PSO have 9.075 s. This substantial reduction in overshoot indicates that the proposed method offers better control and less fluctuation compared to the conventional methods.

Additionally, the proposed method records a peak time of 0.30233 s, which is slightly longer than the peak times of the WNN method (0.30438 s), WNN + LI (0.30229 s), and WNN + PSO (0.30495 s). While the peak time of the proposed method is marginally higher, the dramatic reduction in overshoot highlights its enhanced performance in terms of stability and control response. These results suggest that the WNN + PROP

ijer, 2026, 1, Downloaded from https://onlinelibrary.wiley.com/doi/10.1155/er/2562219 by MS HYEON - Chung-Ang University , Wiley Online Library on [11/03/2026]. See the Terms and Conditions (https://onlinelibrary.wiley.com/terms-and-conditions) on Wiley Online Library for rules of use; OA articles are governed by the applicable Creative Commons License

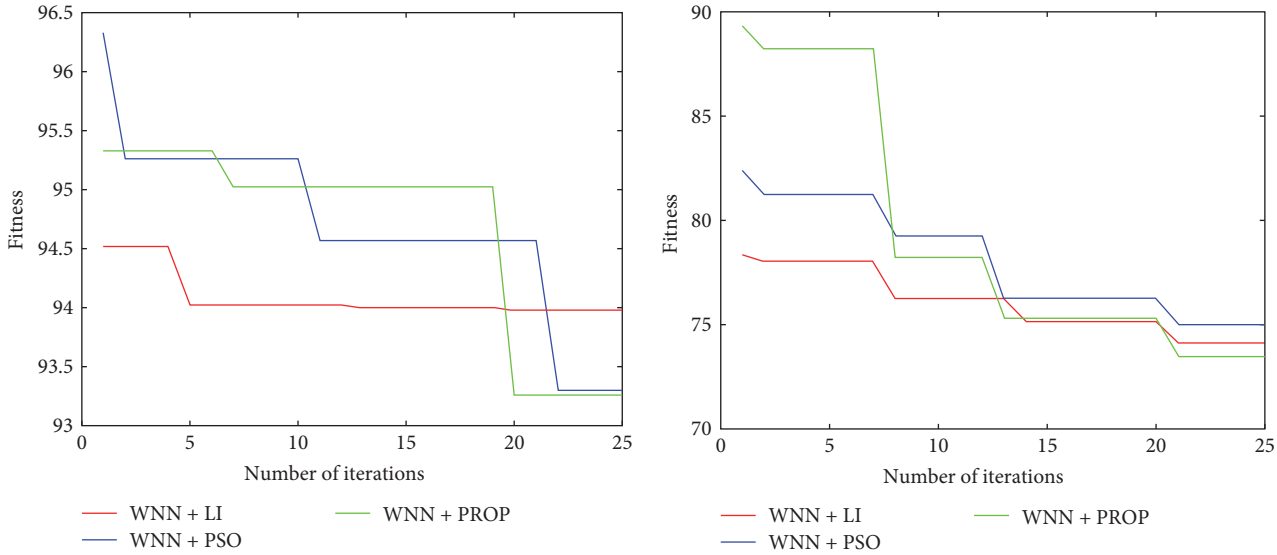


FIGURE 9: Convergence performance comparison with and without load. (a) With load. (b) Without load.

TABLE 3: Error statistics with torque load.

Methods	Best	Worst	Mean	STD
Torque load at 10 N m				
RW-CHO	−1.479	302.06	206.72	100.59
WNN	−1.554	302.18	204.97	101.04
WNN + LI	−1.456	302.06	206.02	100.73
WNN + PSO	−1.498	302.06	206.69	100.67
WNN + PROP	−1.487	301.93	206.74	100.64
Torque load at 5 N m				
WNN	−0.540	302.32	225.45	96.524
WNN + LI	−0.515	302.41	225.45	96.522
WNN + PSO	−0.488	302.41	225.45	96.523
WNN + PROP	−0.521	302.36	225.45	96.523
Torque load at 8 N m				
WNN	−1.0714	302.36	224.92	97.391
WNN + LI	−1.0525	302.43	224.72	97.679
WNN + PSO	−1.0656	302.3	224.98	97.311
WNN + PROP	−1.1072	302.49	224.65	97.741

TABLE 4: Error statistics under no-load condition.

Methods	Best	Worst	Mean	STD
RW-CHO	0	302.4	225.48	96.472
WNN	$-8.20e^{-17}$	302.46	225.48	96.471
WNN + LI	$-4.68e^{-17}$	302.4	225.48	96.472
WNN + PSO	0	302.39	225.48	96.472
WNN + PROP	$-7.74e^{-17}$	302.52	225.48	96.472

method provides a more stable and efficient control strategy, particularly by minimizing overshoot, which is crucial for improving the overall performance of motor control systems under load conditions.

Table 6 presents the stability analysis results under no-load conditions. The proposed WNN + PROP method demonstrates an undershoot of $2.5824e^{-17}$ s, which is significantly lower than the undershoots observed in traditional methods.

ijer, 2026, 1, Downloaded from https://onlinelibrary.wiley.com/doi/10.1155/er/2562219 by MS HYEON - Chung-Ang University , Wiley Online Library on [11/03/2026]. See the Terms and Conditions (https://onlinelibrary.wiley.com/terms-and-conditions) on Wiley Online Library for rules of use; OA articles are governed by the applicable Creative Commons License

Table 5: Stability analysis.

Parameters	RW-CHO	WNN	WNN + LI	WNN + PSO	WNN + PROP
Torque load condition of 10 N m					
Rise time	0.29281	0.29676	0.29436	0.29228	0.29249
Settling time	0.36321	0.36865	0.36478	0.36325	0.36252
Settling min	269.73	270.07	269.62	269.74	269.72
Settling max	302.06	302.18	302.06	302.06	301.93
Overshoot	0.78703	0.70215	0.82916	0.78321	0.74975
Undershoot	0.49376	0.51818	0.48627	0.49982	0.49632
Peak	302.06	302.18	302.06	302.06	301.93
Peak time	0.37611	0.38141	0.37759	0.37624	0.37585
Torque load condition of 5 N m					
Rise time	0.24037	0.24037	0.24024	0.24008	0.24037
Settling time	0.29345	0.29327	0.29338	0.29318	0.29345
Settling min	270.06	270.06	270.12	270.05	270.06
Settling max	302.32	302.41	302.41	302.36	302.32
Overshoot	0.7528	0.78069	0.76014	0.76697	0.7528
Undershoot	0.17997	0.17185	0.1629	0.17392	0.17997
Peak	302.32	302.41	302.41	302.36	302.32
Peak time	0.30322	0.30395	0.3041	0.30425	0.30322
Torque load condition of 8 N m					
Rise time	0.23662	0.23609	0.23677	0.23548	0.23662
Settling time	0.29353	0.29336	0.29348	0.29343	0.29353
Settling min	270.02	270.01	270.01	270	270.02
Settling max	302.36	302.43	302.3	302.49	302.36
Overshoot	0.78003	0.80964	0.76062	0.8329	0.78003
Undershoot	0.35711	0.35084	0.35518	0.36907	0.35711
Peak	302.36	302.43	302.3	302.49	302.36
Peak time	0.30438	0.30229	0.30495	0.30233	0.30438

Table 6: Stability analysis under no-load condition.

Parameters	RW-CHO	WNN	WNN + LI	WNN + PSO	WNN + PROP
Rise time	0.24018	0.24062	0.24019	0.24017	0.24013
Settling time	0.29326	0.29342	0.29329	0.29331	0.29308
Settling min	270.09	270.12	270.09	270.1	270.07
Settling max	302.4	302.46	302.4	302.39	302.52
Overshoot	0.76834	0.7775	0.76802	0.75814	0.81249
Undershoot	0	$2.7327e^{-17}$	$1.5602e^{-17}$	0	$2.5824e^{-17}$
Peak	302.4	302.46	302.4	302.39	302.52
Peak time	0.30382	0.30492	0.304	0.3039	0.30402

For comparison, RW-CHO, WNN, and WNN + PSO all achieve an undershoot of 0 s, while WNN + LI has a slightly lower undershoot of $1.5602e^{-17}$ s. This dramatic reduction in undershoot indicates that the proposed method excels in minimizing deviations from the desired state, ensuring smoother and more stable operation under no-load conditions. Moreover, the proposed approach records a peak value of 302.52 s, which is marginally higher than the peak values of the traditional methods: RW-CHO (302.4 s), WNN (302.46 s), WNN + LI (302.4 s), and WNN + PSO (302.39 s). While the peak value of the proposed method is slightly greater, the overall performance is still very competitive, particularly when considering the significantly lower undershoot achieved. These results highlight the superiority of the WNN + PROP method in terms of minimizing undershoot while maintaining peak values within a comparable range to the traditional approaches. This further emphasizes the proposed method's ability to enhance stability and efficiency in motor control systems, particularly under no-load conditions.

The proposed WNN + PROP method demonstrates superior performance compared to traditional methods such as RW-CHO, WNN, WNN + LI, and WNN + PSO in various motor control scenarios. In terms of response time, the proposed method consistently outperforms conventional approaches,

ijer, 2026, 1, Downloaded from https://onlinelibrary.wiley.com/doi/10.1155/er/2562219 by MS HYEON - Chung-Ang University , Wiley Online Library on [11/03/2026]. See the Terms and Conditions (https://onlinelibrary.wiley.com/terms-and-conditions) on Wiley Online Library for rules of use; OA articles are governed by the applicable Creative Commons License

Table 7: Comparative analysis of speed responses under load and no-load conditions for proposed and traditional models.

Load variation	RW-CHO	WNN	WNN + LI	WNN + PSO	WNN + PROP
Load = 10	206.72	204.97	206.02	206.69	207.74
No load	225.48	225.48	225.48	225.48	225.48

Table 8: Comparative analysis of speed responses under varying load conditions.

Load variation	RW-CHO	WNN	WNN + LI	WNN + PROP
Load = 5	225.98	225.87	225.75	226.45
Load = 8	224.92	224.72	224.98	225.65

achieving faster settling and rise times across different torque loads (10, 5, and 8 N m), as well as under no-load conditions. Specifically, the WNN + PROP method exhibited a settling time of 0.36252 s under a 10 N m load, which is faster than the traditional models. It also achieves lower error statistics and improved stability, with notable reductions in overshoot and undershoots. The method shows enhanced convergence rates, reaching faster results both under loaded and unloaded conditions. Despite a slightly higher peak value in some cases, the proposed method excels in minimizing undershoot and demonstrating better overall dynamic performance. These results validate the WNN + PROP method as an efficient and reliable approach for BLDC motor control systems.

4.7. Comparative Analysis of Speed Responses. Table 7 presents a comparative analysis of the speed responses under load and no-load conditions for the proposed WNN + PROP model against traditional models, including RW-CHO, WNN, WNN + LI, and WNN + PSO. The comparison was conducted with a torque load of 10 N m, and speed measurements were analyzed for each model under both load and no-load conditions. On observing the load condition at 10 N m, the WNN + PROP model provided the highest speed, outperforming RW-CHO (206.72 rpm), WNN (204.97 rpm), WNN + LI (206.02 rpm), and WNN + PSO (206.69 rpm). These findings indicate that the WNN + PROP model offers the fastest response under load conditions. In contrast, under the no-load condition, all models exhibited identical speeds of 225.48 rpm. Overall, the comparison highlights that the WNN + PROP model achieves superior speed performance under load conditions compared to traditional models. This result shows the effectiveness and accuracy of the WNN + PROP model when compared to traditional methods.

4.8. Comparative Analysis of Speed Responses Under Varying Load. The results presented in Table 8, show the speed responses of the RW-CHO, WNN, WNN + LI, and WNN+PSO, models under two different torque load conditions: 5 and 8 N m. On observing the result at a 5 N m load, the proposed RW-CHO model exhibited the highest speed response of 226.45 rpm, when compared with the WNN (225.75 rpm), WNN + LI (225.87 rpm), and RW-CHO (225.98 rpm) models. Similarly, for the load of 8 N m, the proposed RW-CHO model shows the highest speed response of 225.65 rpm, outperforming WNN (224.98 rpm), WNN + LI (224.72 rpm), and RW-CHO (224.92 rpm).

These findings suggest that the proposed WNN + PROP model offers better speed performance under varying load conditions, outperforming the traditional models. This result demonstrates the effectiveness and improved speed response capability of the proposed WNN + PROP model compared to traditional methods like RW-CHO, WNN and WNN + LI.

5. Conclusions

This study introduces an innovative WNN integrated with an optimized FOPID controller for sensorless speed control of BLDC motors. The FOPID controller's gain variables are optimized using a novel meta-heuristic algorithm, RW-CHO, offering substantial advantages, such as faster convergence and improved efficiency. This approach achieves high precision with less iteration than traditional methods. Simulation results confirm that the WNN-FOPID controller outperforms existing techniques like RW-CHO, WNN, WNN + LI, and WNN + PSO in both loaded and no-load conditions. It demonstrates enhanced control over key performance metrics, including rise time, peak time, settling time, and error statistics across various operating scenarios. The proposed method can be applied in fields requiring precise and reliable speed control of BLDC motors, such as in EVs, robotics, and industrial automation systems. Future research could focus on integrating deep learning techniques for fault detection and diagnostics, enabling proactive maintenance and adaptive control adjustments, and ensuring long-term reliability and performance optimization in BLDC motor drives. Additionally, the future direction of this study may involve incorporating hardware setups for hardware validation.

Nomenclature

WNN:	Wavelet neural network
WN:	Wavelet network
ANN:	Artificial neural network
RW-CHO:	Random weighted chimp optimization
PID:	Proportional integral derivative
FOPID:	Fractional-order proportional integral derivative
ANFIS:	Adaptive neural fuzzy inference system
ChOA:	Chimp optimization algorithm
MLP:	Multilayer perceptron topology
LSO:	Lion swarm optimization
GPFOPI:	Generalized predictive fractional-order PI

ijer, 2026, 1, Downloaded from https://onlinelibrary.wiley.com/doi/10.1155/er/2562219 by MS HYEON - Chung-Ang University , Wiley Online Library on [11/03/2026]. See the Terms and Conditions (https://onlinelibrary.wiley.com/terms-and-conditions) on Wiley Online Library for rules of use; OA articles are governed by the applicable Creative Commons License

TID:	Tilt integral derivative controller
CATSCG:	Chaotic adaptive tuning strategy for controller gain
CODE:	Chaotic online differential evolution
PSO:	Particle swarm optimization
PI:	Proportional integral
SREH∞F:	Square-root extended *H*∞ filter
EMF:	Electromagnetic force.

Data Availability Statement

The data will be made available upon request.

Conflicts of Interest

The authors declare no conflicts of interest.

Author Contributions

Methodology, writing – original draft: D. S. Purushothaman and K. R. Santha. Writing – review and editing, formal analysis: Mohammed H. Alsharif and Mun-Kyeom Kim.

Funding

This research was supported by the Chung-Ang University Research in 2025 (Grant Number: CAU-2025).

References

[1] A. Ramya, M. Balaji, and V. Kamaraj, "Adaptive MF Tuned Fuzzy Logic Speed Controller for BLDC Motor Drive Using ANN and PSO Technique," *The Journal of Engineering* 2019, no. 17 (2019): 3947–3950.

[2] D. Chowdhury, M. Chattopadhyay, and P. Roy, "Modelling and Simulation of Cost Effective Sensorless Drive for Brushless DC Motor," *Procedia Technology* 10 (2013): 279–286.

[3] T.-H. Kim and M. Ehsani, "Sensorless Control of the BLDC Motors From Near-Zero to High Speeds," *IEEE Transactions on Power Electronics* 19, no. 6 (2004): 1635–1645.

[4] D.-K. Kim, K.-W. Lee, and B.-I. Kwon, "Commutation Torque Ripple Reduction in a Position Sensorless Brushless DC Motor Drive," *IEEE Transactions on Power Electronics* 21, no. 6 (2006): 1762–1768.

[5] J. C. Gamazo-Real, E. Vázquez-Sánchez, and J. Gómez-Gil, "Position and Speed Control of Brushless DC Motors Using Sensorless Techniques and Application Trends," *Sensors* 10, no. 7 (2010): 6901–6947.

[6] M. Akrami, E. Jamshidpour, B. Nahid-Mobarakeh, S. Pierfederici, and V. Frick, "Sensorless Control Methods for BLDC Motor Drives: A Review," *IEEE Transactions on Transportation Electrification* (2024).

[7] B. Saha, B. Singh, and A. Sen, "SMO Based Position Sensorless BLDC Motor Drive Employing Canonical Switching Cell Converter for Light Electric Vehicle," *IEEE Transactions on Industry Applications* 59, no. 3 (2023): 2974–2984.

[8] M. Sundaram, J. Chelladurai, M. Anand, M. S. S. Kumari, S. Sharma, and M. E. H. Assad, "A Novel Approach to Energy-Optimized Variable-Speed Sensorless-Based Brushless DC Motors (BLDC) Control for Automotive Wiper Applications," *Arabian Journal for Science and Engineering* 49, no. 2 (2024): 1491–1504.

[9] B. Saha, A. Sen, B. Singh, K. Mahtani, and J. A. Sánchez-Fernández, "Quadrature-Phase-Locked-Loop-Based Back-Electromotive Force Observer for Sensorless Brushless DC Motor Drive Control in Solar-Powered Electric Vehicles," *Applied Sciences* 15, no. 2 (2025): 574.

[10] K. Premkumar and B. V. Manikandan, "Adaptive Neuro-Fuzzy Inference System Based Speed Controller for Brushless DC Motor," *Neurocomputing* 138 (2014): 260–270.

[11] N. Saed and M. Mirsalim, "Enhanced Sensor-Less Speed Control Approach Based on Mechanical Offset for Dual-Stator Brushless DC Motor Drives," *IET Electric Power Applications* 14, no. 5 (2020): 885–892.

[12] R. Shanmugasundram, K. M. Zakaraiah, and N. Yadaiah, "Modeling, Simulation and Analysis of Controllers for Brushless Direct Current Motor Drives," *Journal of Vibration and Control* 19, no. 8 (2013): 1250–1264.

[13] V. Verma, N. S. Pal, and B. Kumar, "Speed Control of the Sensorless BLDC Motor Drive Through Different Controllers", in *Harmony Search and Nature Inspired Optimization Algorithms*, (Springer, Singapore, 2019): 143–152.

[14] M.-S. Wang, S.-C. Chen, and C.-H. Shih, "Speed Control of Brushless DC Motor by Adaptive Network-Based Fuzzy Inference," *Microsystem Technologies* 24, no. 1 (2018): 33–39.

[15] X. Z. Zhang and Y. N. Wang, "A Novel Position-Sensorless Control Method for Brushless DC Motors," *Energy Conversion and Management* 52, no. 3 (2011): 1669–1676.

[16] M. Zhao, X. Liu, and H. Su, "Robust Adaptive Speed Control of Disturbed Brushless Direct Current Motor," in *2017 Eighth International Conference on Intelligent Control and Information Processing (ICICIP)*, (Hangzhou, China, 2017), 141–146.

[17] R. Pindoriya, S. Rajendran, and P. Chauhan, "Speed Control of BLDC Motor Using PWM Technique," *International Journal of Advance Engineering and Research Development (IJAERD)* 4, no. ETCEE-2014 Issue (2014): 18–21.

[18] D. S. Purushothaman and K. R. Santha, "Artificial Neural Network With Optimized FOPID for Speed Control of Sensorless BLDC Motor Drive," *Cybernetics and Systems* (2022): 1–23.

[19] G. Yao, J. Feng, G. Wang, and S. Han, "BLDC Motors Sensorless Control Based on MLP Topology Neural Network," *Energies* 16, no. 10 (2023): 4027.

[20] T. Wang, H. Wang, H. Hu, J. Qing, and C. Wang, "Lion Swarm Optimisation-Based Tuning Method for Generalised Predictive Fractional-Order PI to Control the Speed of Brushless Direct Current Motor," *IET Electric Power Applications* 16, no. 8 (2022): 879–895.

[21] K. Sayed, H. H. El-Zohri, A. Ahmed, and M. Khamies, "Application of Tilt Integral Derivative for Efficient Speed Control and Operation of BLDC Motor Drive for Electric Vehicles," *Fractal and Fractional* 8, no. 1 (2024): 61.

[22] K. Kroičs and A. Būmanis, "BLDC Motor Speed Control With Digital Adaptive PID-Fuzzy Controller and Reduced Harmonic Content," *Energies* 17, no. 6 (2024): 1311.

[23] K. P. B. Chandra, D. Potnuru, D. Durairaj, P. Manoharan, and H. H. Alhelou, "Nonlinear State Estimator Design and Implementation for Speed Control of a BLDC Motor Drive Using Square-Root Extended H∞ H_∞ Filter," *IET Power Electronics* 16, no. 13 (2023): 2249–2260.

[24] A. Rodríguez-Molina, M. G. Villarreal-Cervantes, O. Serrano-Pérez, J. Solís-Romero, and R. Silva-Ortigoza, "Optimal Tuning of the Speed Control for Brushless DC Motor Based on Chaotic

ijer, 2026, 1, Downloaded from https://onlinelibrary.wiley.com/doi/10.1155/er/2562219 by MS HYEON - Chung-Ang University , Wiley Online Library on [11/03/2026]. See the Terms and Conditions (https://onlinelibrary.wiley.com/terms-and-conditions) on Wiley Online Library for rules of use; OA articles are governed by the applicable Creative Commons License

Online Differential Evolution," *Mathematics* 10, no. 12 (2022): 1977.
[25] A. Intidam, H. El Fadil, H. Housny, et al., "Development and Experimental Implementation of Optimized PI-ANFIS Controller for Speed Control of a Brushless DC Motor in Fuel Cell Electric Vehicles," *Energies* 16, no. 11 (2023): 4395.
[26] S. S. A. Naqvi, H. Jamil, N. Iqbal, et al., "Multi-Objective Optimization of PI Controller for BLDC Motor Speed Control and Energy Saving in Electric Vehicles: A Constrained Swarm-Based Approach," *Energy Reports* 12 (2024): 402–417.
[27] M. A. Baba, M. Naoui, and M. Cherkaoui, "Modeling and Simulation of a BLDC Motor Speed Control in Electric Vehicles," in *International Conference on Digital Technologies and Applications*, (Cham: Springer Nature Switzerland, 2023), 883–895.
[28] O.-D. Ramírez-Cárdenas and F. Trujillo-Romero, "Sensorless Speed Tracking of a Brushless DC Motor Using a Artificial Neural Network," *Mathematical and Computational Applications* 25, no. 3 (2020): 57.
[29] R. Ganesan, S. Suresh, and S. S. Sivaraju, "ANFIS Based Multi-Sector Space Vector PWM Scheme for Sensorless BLDC Motor Drive," *Microprocessors and Microsystems* 76 (2020): 103091.
[30] J.-Y. Cao, J. Liang, and B.-G. Cao, "Optimization of Fractional-Order PID Controllers Based on Genetic Algorithms," in *IEEE International Conference on Machine Learning and Cybernetics*, (Guangzhou, China: IEEE, 2005).
[31] M. C. Bhuvaneswari and J. Saxena, "Lecture Notes in Electrical Engineering," *Intelligent and Efficient Electrical Systems* 446 (2018): 117–127.
[32] F. Padula and A. Visioli, "Tuning Rules for Optimal PID and Fractional-Order PID Controllers," *Journal of Process Control* 21, no. 1 (2011): 69–81.
[33] A. A. Kesarkar and N. Selvaganesan, "Tuning of Optimal Fractional-Order PID Controller Using an Artificial Bee Colony Algorithm," *Systems Science and Control Engineering* 3, no. 1 (2015): 99–105.
[34] Q. Zhang and A. Benveniste, "Wavelet Networks," *IEEE Transactions on Neural Networks* 3, no. 6 (1992): 889–898.
[35] G. Wang, L. Guo, and H. Duan, "Wavelet Neural Network Using Multiple Wavelet Functions in Target Threat Assessment," *The Scientific World Journal* 2013, no. 1 (2013): 632437.
[36] M. Khishe and M. R. Mosavi, "Chimp Optimization Algorithm," *Expert Systems With Applications* 149 (2020): 113338.

ijer, 2026, 1, Downloaded from https://onlinelibrary.wiley.com/doi/10.1155/er/2562219 by MS HYEON - Chung-Ang University , Wiley Online Library on [11/03/2026]. See the Terms and Conditions (https://onlinelibrary.wiley.com/terms-and-conditions) on Wiley Online Library for rules of use; OA articles are governed by the applicable Creative Commons License